Interior Target Tracking Using Digital Communications Signals for Bistatic Radar using Gnu Radio

Todd K. Moon TODD.MOON@USU.EDU
Electrical and Computer Engineering
Utah State University

Thomas Bradshaw TBRADSH@SANDIA.GOV
Utah State University

Abstract

Wireless communication systems employed in buildings (such as WiFi) can be used for bistatic radar to track targets moving in the building. The transmit and receive hardware and software can be readily implemented using Gnu radio. The general processing steps at the receive include Doppler frequency extraction, using FFT or MUSIC-algorithm based processing, following by Viterbi or BCJR algorithm to smooth the frequency trajectory, followed by track extraction using an extended Kalman filter. The method has been implemented and tested using real hardware.

1. Introduction

The wireless communications equipment now common in buildings (e.g., WiFi) can be alternatively utilized in a bistatic radar configuration to track targets moving in the building, and to the presence of intruders. This opens new possibilities for surveillance and securing of both residential and commercial buildings with little additional infrastructure. The method uses additional antennas (for tracking purposes), but for the intrusion detection only a single receive antenna may be necessary.

Figure 1 illustrates the concept at a high level. In this prototype system there is a single moving target at location $\mathbf{g}(t) = (x(t), y(t))$. There is a transmitter antenna at location $\mathbf{t}_1 = (x_{t,1}(t), y_{t,1}(t))$. (Typically the transmitter is fixed, but it could be moving.) There are also a series of J receive antennas spatially distributed around the area over which surveillance is desired, at locations $\mathbf{q}_1(t), \ldots, \mathbf{q}_J(t)$. These antennas are also typically fixed. There is a direct transmission path from the transmitter to a receiver. The transmitted signal also reflects off the moving target and is also received at the receive antenna. The receive antenna thus receives the sum of the direct path signal and the reflected signal, each delayed due to the propagation distances involved. The distance (range) from transmitter to the target is $R_{T,1}(t)$. The distance from target to receiver j is $R_{R,j}(t)$. Due to the motion of the target relative to the transmit and receive antennas, producing changes in $R_{T,1}(t)$ and $R_{T,j}(t)$, the reflected component is Doppler shifted. This scenario is, in fact, very common, and WiFi receivers deal with the reflected path signals that they receive fairly effortlessly using their internal signal processing (e.g., symbol timing estimation, phase locked loops, equalization) because reflected path signals tend to be weak, so the receiver effectively compensates for the reflected signal component.

In our case, however, it is precisely the reflected signal component that is of interest. The receiver system does signal processing to separate the reflected path signal component from the direct path, and then estimates the Doppler frequencies from the reflected path component. The Doppler frequency estimates from each antenna are then used in an extended Kalman filter, which fuses the information together to estimate the position $(x(t), y(t))$ and velocity $(v_x(t), v_y(t))$ of the target.

The system thus described has been prototyped using Gnu radio and Ettus hardware components to build the transmitter and receivers. For the prototype, a QPSK transmitter has been used. We are moving toward implementing the system on WiFi signals. For development of the tracking algorithms, signals acquired using Gnu radio are further processed using Matlab to extract the Doppler and tracking information. Figure 2 shows a block diagram of the operation.

This paper presents results developed by (Bradshaw, 2021). Further details on parameter settings and experimental results can be found in that thesis, which can be found at `https://engineering.usu.edu/`

Proceedings of the 1st GNU Radio Conference, Copyright 2016 by the author(s).

ece/research/publications/thesis-sort.

By exploiting an RF signal as a it is possible to overload an additional function of target tracking by creating a bistatic radar system (radar in which the transmitter and receiver are in different locations). A significant difference between this system and more conventional bistatic radars is that in conventional bistatic radar there is a direct measurement of the transmitted signal, whereas in this system there is no direct measurement of the transmitted signal. The fact that the signal is a digital communication signal allows information about the reflected signal to be extracted.

2. Signal and Gnu Radio Components

A key aspect in separating the direct and reflected signals is that the signals employ digital communication. The transmitted signal is assumed to be a bandpass digital communications signal of the form

$$s(t) = A(t)e^{\jmath(2\pi f_c(t)t+\phi(t))} = e^{\jmath 2\pi f_c(t)} \sum_k a_k p(t-kT_s).$$

For purposes here this a single-carrier QAM signal, but the methods here can be extended to multicarrier OFDM signals as well. Here $\jmath$ is the complex unit and $f_c(t)$ is the carrier frequency. It is portrayed here as time-varying to represent the fact that in the Ettus hardware used there is carrier frequency drift at both the transmitter and receiver, compensating for which represented a significant practical challenge. a_k is the complex symbol at the kth symbol time, $p(t)$ is the pulse shape (e.g., square root raised cosine), and T_s is the symbol time.

The signal for our prototype/testing system employs QPSK modulation. A Gnu radio flowgraph for the transmitter appears in the top half of figure 3.

Let $\tau_{1,j}$ denote the time delay from transmitter at $\mathbf{t}_1$ to receiver at $\mathbf{q}_j$. Let $\tilde{\tau}_{1,j}$ denote the total delay on the reflected path from $\mathbf{t}_1$ to $\mathbf{g}(t)$ then to $\mathbf{q}_j$. Due to the physical dimensions (transmission inside a building) and typical transmission rates, it is assumed that $p(t-\tau_{1,j}) \approx p(t-\tilde{\tau}_{1,j})$, that is, the additional delay on the reflected path is much less than a symbol time. The received signal is basebanded using a local carrier $\hat{f}_c(t)$. Since in general the transmitter and receiver carrier clocks are distinct, we specifically do not assume that $f_c(t) = \hat{f}_c(t)$. In experiments using real hardware, we have found that the carrier frequency offsets fall in roughly the same frequency range as the Doppler frequencies from targets moving in a building. The basebanded received signal (neglecting noise) can be written as

$$w_{1,j}(t) = \alpha_{1,j} A(t-\tau_{1,j}) e^{\jmath(2\pi f_c(-\tau_{1,j})+\phi(t-\tau_{1,j})+tf_e(t))}$$
$$+ \tilde{\alpha}_{1,j} A(t-\tilde{\tau}_{1,j}) e^{\jmath(2\pi(f_c(-\tilde{\tau}_{1,j})-f_{d,i,j}(t-\tilde{\tau}_{1,j}))+\phi(t-\tilde{\tau}_{1,j})+tf_e(t))} \tag{1}$$

$$\approx \alpha_{1,j} A(t) e^{\jmath(\phi(t)+tf_e(t)} + \tilde{\alpha}_{1,j} A(t) e^{\jmath(\phi(t)+f_{d,1,j}(t)t+tf_e(t))} \tag{2}$$

Here, $f_e(t) = f_c(t) - \hat{f}_c(t)$ represents the carrier frequency offset at the receiver. The complex factor $\alpha_{1,j}$ represents the attenuation and phase of the signal on the path from transmitter i to receiver j; $\tilde{\alpha}_{1,j}$ represents the attenuation and phase on the path from transmitter to target to receiver. Fixed phase factors from (1) and phase factors due to the change of variables have been absorbed into $\alpha_{1,j}$ and $\tilde{\alpha}_{1,j}$ in (2). Due to the weakness of the reflected signal, $|\tilde{\alpha}_{1,j}| \ll |\alpha_{1,j}|$, so the reflected signal affects the received signal as a small additional contribution to the noise. In an indoor setting, $|\tilde{\alpha}_{1,j}|$ is 10 to 15 dB smaller than $|\alpha_{1,j}|$.

For now, focus on a single transmission channel and write $\alpha_{1,j} = \alpha$; similarly for $\tilde{\alpha}_{1,j}$ and $f_{d,1,j}$. The output of the symbol timing/matched filter for the kth symbol (prior to a PLL) can be written as

$$y_k = a_k(\alpha + \tilde{\alpha} e^{\jmath 2\pi f_{d,k} k}) e^{\jmath 2\pi f_{e,k} k} + \text{noise}$$

Here $f_{d,k}$ is the time-varying Doppler frequency per symbol. Since the reflected component is weak, the symbol a_k can be detected at the receiver in the usual way, since the reflected path component $\tilde{\alpha} e^{\jmath 2\pi f_{d,k} k} e^{\jmath 2\pi f_{e,k} k}$ simply acts as a fairly insignificant additional noise component. This signal can be passed through a PLL (to track/remove the carrier frequency offset) and the symbol can be detected. The presence of the reflected path component affects the PLL usually insignificantly since $|\tilde{\alpha}| \ll |\alpha|$. A Gnu radio flowgraph showing this detection is shown in figure 3, including the Carrier Phase Synchronizer" and the “QPSK Symbol Detection”. Let $\hat{a}_k$ denote the detected symbol. The transmitted signal is removed from the matched filter output to form the signal

$$d_2(k) = \frac{y_k}{\hat{a}_k} \approx (\alpha + \tilde{\alpha} e^{j 2\pi f_{d,k} k}) e^{j 2\pi f_{e,k} k} + \text{noise}.$$

This is performed by the Gnu radio flowgraph shown in figure 3, the portion labeled “Note: D2”. It is by this means that the direct path and reflected path components are separated. In the Gnu radio flowgraph, the data $d_2(k)$ are saved to a file, and in our prototype system the remaining signal processing is accomplished using Matlab.

3. Doppler Frequency Extraction

The Matlab code performs the following operations.

Carrier frequency offset estimation. As mentioned, the hardware used has significant carrier frequency offsets. In

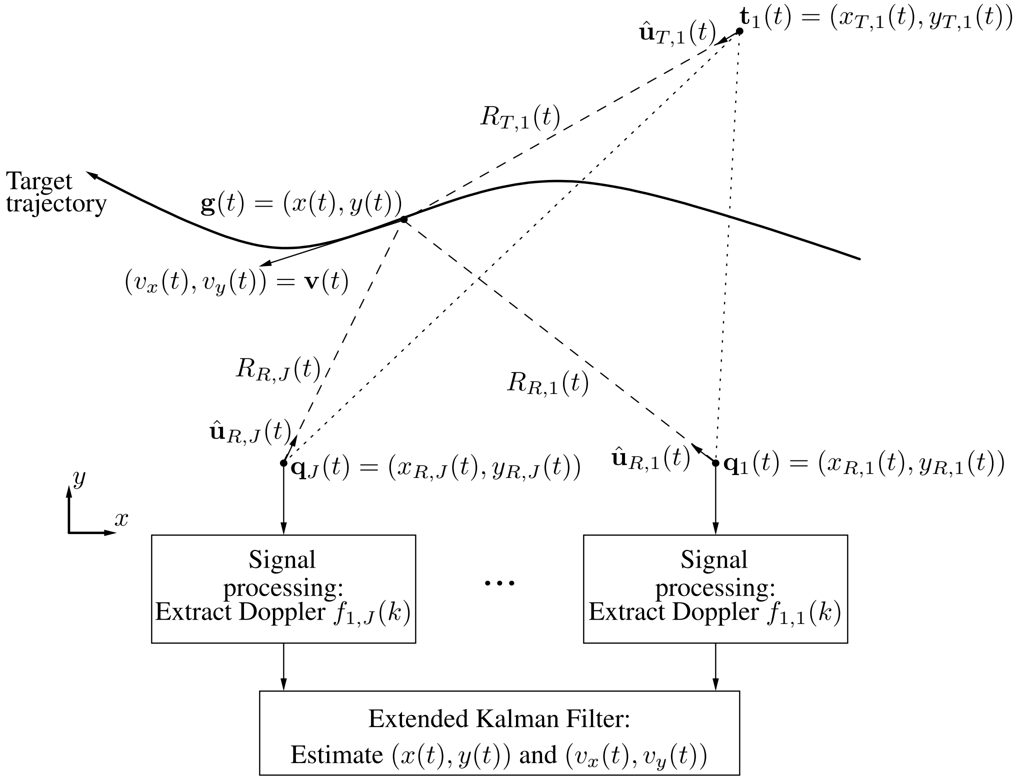
$\hat{\mathbf{u}}_{T,1}(t)$
$\mathbf{t}_1(t) = (x_{T,1}(t), y_{T,1}(t))$
$R_{T,1}(t)$
Target trajectory
$\mathbf{g}(t) = (x(t), y(t))$
$(v_x(t), v_y(t)) = \mathbf{v}(t)$
$R_{R,J}(t)$
$R_{R,1}(t)$
$\hat{\mathbf{u}}_{R,J}(t)$
$\mathbf{q}_J(t) = (x_{R,J}(t), y_{R,J}(t))$
$\hat{\mathbf{u}}_{R,1}(t)$
$\mathbf{q}_1(t) = (x_{R,1}(t), y_{R,1}(t))$
y
x
Signal processing: Extract Doppler $f_{1,J}(k)$
...
Signal processing: Extract Doppler $f_{1,1}(k)$
Extended Kalman Filter: Estimate $(x(t), y(t))$ and $(v_x(t), v_y(t))$

Figure 1. Configuration of a bistatic target tracking system

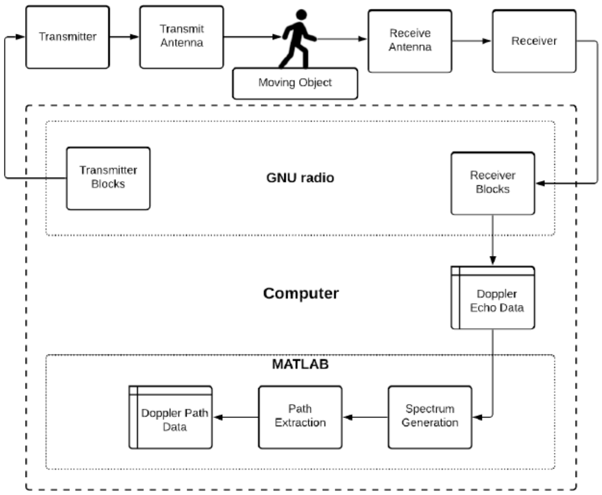

Figure 2. System block diagram

$d_2(k)$, the term with carrier frequency offset, $\alpha e^{j2\pi f_e k}$, is much stronger than the reflected path component. Spectral estimation is performed using FFTs or the MUSIC algorithm (Schmidt, 1979; Moon & Stirling, 2000). Even though only a single signal component is present, the MUSIC algorithm was explored using different numbers of signal and noise components. It was found that better spectral estimates were obtained using a much larger noise space than would be assumed necessary (approximately 50 dimensions).

Carrier frequency offset removal; Mean removal. The estimated carrier frequency offset $\hat{f}_e(t)$ is used to baseband $d_2(k)$. The resulting direct-path component α is removed by computing the mean over a block and subtracting it. Note that this mean removal step has the effect of also removing the reflected path Doppler when it is at 0 Hz.

Doppler frequency Estimation. The Doppler frequency sequence is estimated using the mean-removed signal from the previous step using either FFT or MUSIC algorithm. This estimate is problematic when the Doppler frequency falls near 0, since that component is eliminated by the mean removal step.

Spectral estimate smoothing: Viterbi or BCJR. From physical considerations, the Doppler frequencies form a

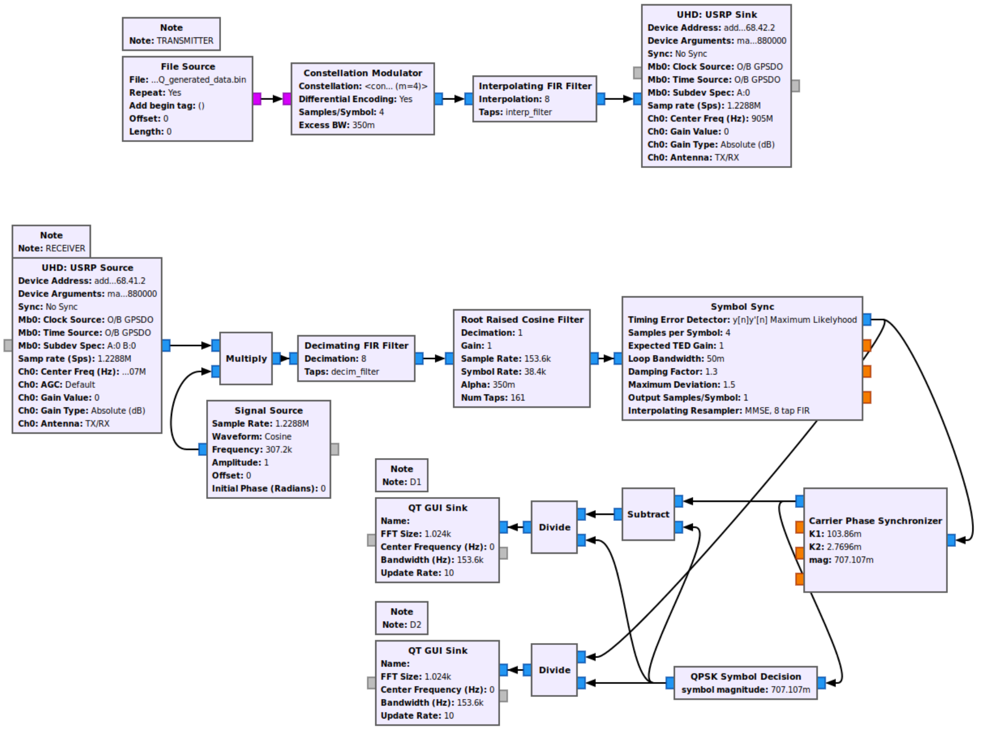

Note
Note: TRANSMITTER

File Source
File: ...Q_generated_data.bin
Repeat: Yes
Add begin tag: ()
Offset: 0
Length: 0

Constellation Modulator
Constellation: <con... (m=4)>
Differential Encoding: Yes
Samples/Symbol: 4
Excess BW: 350m

Interpolating FIR Filter
Interpolation: 8
Taps: interp_filter

UHD: USRP Sink
Device Address: add...68.42.2
Device Arguments: ma...880000
Sync: No Sync
Mb0: Clock Source: O/B GPSDO
Mb0: Time Source: O/B GPSDO
Mb0: Subdev Spec: A:0
Samp rate (Sps): 1.2288M
Ch0: Center Freq (Hz): 905M
Ch0: Gain Value: 0
Ch0: Gain Type: Absolute (dB)
Ch0: Antenna: TX/RX

Note
Note: RECEIVER

UHD: USRP Source
Device Address: add...68.41.2
Device Arguments: ma...880000
Sync: No Sync
Mb0: Clock Source: O/B GPSDO
Mb0: Time Source: O/B GPSDO
Mb0: Subdev Spec: A:0 B:0
Samp rate (Sps): 1.2288M
Ch0: Center Freq (Hz): ...07M
Ch0: AGC: Default
Ch0: Gain Value: 0
Ch0: Gain Type: Absolute (dB)
Ch0: Antenna: TX/RX

Multiply

Signal Source
Sample Rate: 1.2288M
Waveform: Cosine
Frequency: 307.2k
Amplitude: 1
Offset: 0
Initial Phase (Radians): 0

Decimating FIR Filter
Decimation: 8
Taps: decim_filter

Root Raised Cosine Filter
Decimation: 1
Gain: 1
Sample Rate: 153.6k
Symbol Rate: 38.4k
Alpha: 350m
Num Taps: 161

Symbol Sync
Timing Error Detector: y[n]y'[n] Maximum Likelyhood
Samples per Symbol: 4
Expected TED Gain: 1
Loop Bandwidth: 50m
Damping Factor: 1.3
Maximum Deviation: 1.5
Output Samples/Symbol: 1
Interpolating Resampler: MMSE, 8 tap FIR

Note
Note: D1

QT GUI Sink
Name:
FFT Size: 1.024k
Center Frequency (Hz): 0
Bandwidth (Hz): 153.6k
Update Rate: 10

Divide

Subtract

Carrier Phase Synchronizer
K1: 103.86m
K2: 2.7696m
mag: 707.107m

Note
Note: D2

QT GUI Sink
Name:
FFT Size: 1.024k
Center Frequency (Hz): 0
Bandwidth (Hz): 153.6k
Update Rate: 10

Divide

QPSK Symbol Decision
symbol magnitude: 707.107m

Figure 3. Gnu flowgraph for transmitter and receiver

signal that is continuous in time. In practice, from noise on the signal or from frequency offset estimation errors or Doppler frequency estimation errors, the sequence of Doppler frequency estimates may not be continuous. The constraint of continuity can be imposed to improve the frequency estimate.

This has been done in two ways. The first makes use of the familiar Viterbi algorithm (Forney, 1973; Moon, 2005). A trellis is established over a frequency range $[f_{\min}, f_{\max}]$, with frequency spacing at some quantization. Transitions in the trellis are assumed between only near neighbors in the trellis. Let $v_t(k)$ denote the frequency spectrum for a segment of signal at some time block indexed by time t at frequency index k (e.g., an FFT spectrum, or a MUSIC spectrum). A Viterbi branch metric from frequency state j to frequency state k is defined by

$$\mu(k,j) = \begin{cases} |v_t(k)| - K|k-j| & |k-j| < \delta \\ 0 & \text{otherwise.} \end{cases}$$

Here, $K|k-j|$ is a penalty term that counts large frequency transitions as being less desirable, where K is a weight. δ is a maximum allowable frequency change in a single step. The Viterbi algorithm finds the maximum value path through a trellis of candidate frequency values.

Figure 4 illustrates how the Viterbi algorithm improves the spectrum (on artificial data). Figure 4(a) shows the music spectrum (background) and the maximum MUSIC spectrum points (red). Observe that there are points which fall off (discontinuously) from the apparent signal trajectory. Figure 4(b) shows the result of processing the MUSIC spectrum using the Viterbi algorithm. The path is more continuous, with fewer outliers.

The BCJR algorithm can also be used to smooth the spectrum. The BCJR algorithm (Bahl et al., 1974; Moon, 2005) is a forward/backward algorithm in which effects of information at a state at time t are taken into consideration. The BCJR algorithm returns a probability map, indicating the probability that the state (the frequency estimate in this case) falls into a particular frequency bin. Analogous to the branch cost function of the Viterbi algorithm, the BCJR algorithm has a state transition cost function $\gamma(k,j)$, which can be defined in this case as

$$\gamma(k,j) = \begin{cases} e^{K_2|X(k)|} e^{-K_1|k-j|} & \text{if } |k-j| < \delta \\ 0 & \text{otherwise.} \end{cases}$$

Dealing with the Zero Frequency Removal As mentioned above, the mean removal operation also removes zero frequencies from the Doppler-shifted reflected path, so that $v_t(f)$ does not contribute to good Viterbi paths at $f = 0$. When the Doppler is zero for several branches, it is difficult for the Viterbi algorithm to cross the zero frequency gulf. This can be ameliorated using a *balance fac-*

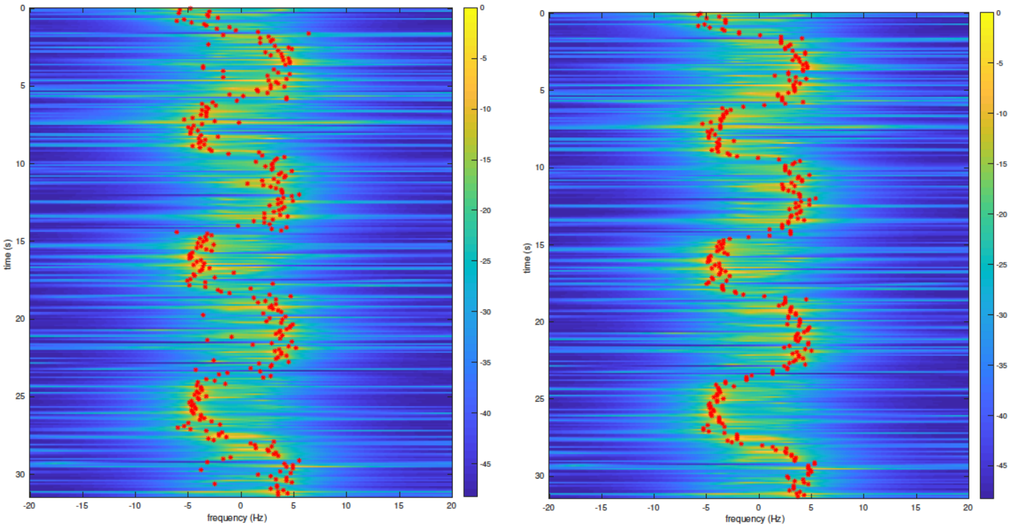

(a) MUSIC spectrum and maximum spectrum points

(b) Result of processing the MUSIC algorithm using the Viterbi algorithm

Figure 4. Illustration of improvement of spectrum estimation using Viterbi algorithm

tor (BF) in conjunction with an *adjustment spectrum*. The balance factor is a measure of how the frequency energy is distributed across the frequencies. It is computed by

$$BF(t) = \frac{\sum_0^{f_{\max}} |v_t(f)| - \sum_{f_{\min}}^0 |v_t(f)|}{\sum_{f_{\min}}^{f_{\max}} |v_t(f)|}$$

The balance factor is in the range $[-1, 1]$. Balance factors hover near 0 when the Doppler frequency is near 0, even if $v_t(0)$ is 0. The balance factor thus provides a sort of surrogate which can be used to compensate for mean-removed frequencies.

Figure 5 illustrates the BF computed for a time-varying signal, artificially scaled to overlay the spectrogram. It can be see that the balance factor closely corresponds to the spectrum, even near 0 frequency.

The balance factor can be used to help the Viterbi (or BCJR) algorithm to tend toward the 0 frequency state by restoring artificial spectral energy near the zero frequency. An *adjustment spectrum* is defined by

$$v_0(f) = \begin{cases} \Lambda - K_3|f| & \text{if} |f| < \sigma \\ 0 & \text{otherwise.} \end{cases}$$

Here Λ is a peak value, and σ is a threshold value. An example adjustment spectrum is shown in figure 6. The *adjusted spectrum* is determined as a linear combination of the spectrum $v_t(f)$ and $v_0(f)$. Let $\tilde{BF}(t) = K_0|BF(t)|$ for a scale factor K_0.

When the balance factor is sufficiently large, $|BF(t)| > \epsilon$, then the measured spectrum $v_t(f)$ can be used. Otherwise,

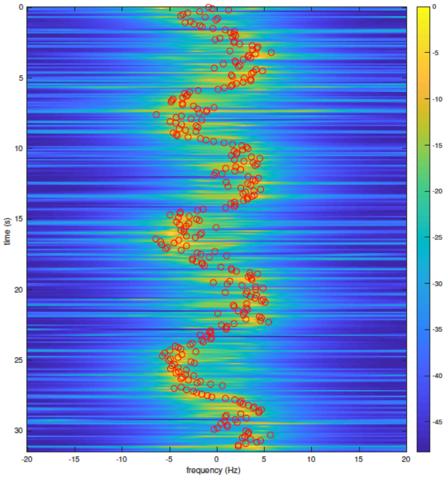

Figure 5. Example scaled balance factor applied to a signal with time-varying spectrum

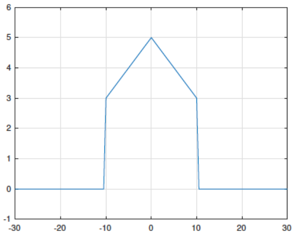

Figure 6. Example adjustment spectrum

an adjust spectrum is obtained as a linear combination of the measured spectrum and the adjusted spectrum. From this, the branch metric is defined as

$$\mu(k,j)=\begin{cases} K_2 v_t(k) - K_1|k-j| \\ \qquad \text{if } |k-j| < \delta \text{ and } BF(t) > \epsilon \\ K_2(B\tilde{F}(t)v_t(k)+(1-B\tilde{F}(t))v_0(k)-K_1|k- \; j| \\ \qquad \text{if}|k-j| < \delta \text{ and } |BF(t)| \leq \epsilon \\ 0 \\ \qquad \text{otherwise.} \end{cases}$$

An exponentiated form can be used to form the state transition cost function for the BCJR algorithm.

4. Motion Model and Extended Kalman Filter

The state of the target is related to the Doppler frequencies as follows. The Doppler frequency at receiver j from the transmitter produced by the relative motion of the transmitter, target, and receiver is (Willis, 1991)

$$f_{d,1,j}(t) = -\frac{1}{\lambda}\left(\frac{dR_{T,1}(t)}{dt} + \frac{dR_{R,j}(t)}{dt}\right) \tag{3}$$

The change in distance depends on the radial component of motion between transmitter/target and target/receiver, so that, using the notation from figure 1,

$$\begin{aligned} &f_{d,1,j}(x(t),y(t),v_x(t),v_y(t)) = \\ &-\frac{1}{\lambda}\Bigg[(v_x(t),v_y(t))\cdot\Bigg(\frac{(x(t),y(t))-(x_{T,1}(t),y_{T,1}(t))}{\|(x(t),y(t))-(x_{T,1}(t),y_{T,1}(t))\|}+ \\ &\qquad\frac{(x(t),y(t))-(x_{R,j}(t),y_{R,j}(t))}{\|(x(t),y(t))-(x_{R,j}(t),y_{R,j}(t))\|}\Bigg) \\ &-(v_{T,1,x}(t),v_{T,1,y}(t))\cdot\frac{(x(t),y(t))-(x_{T,1}(t),y_{T,1}(t))}{\|(x(t),y(t))-(x_{T,1}(t),y_{T,1}(t))\|} \\ &-(v_{R,j,x}(t),v_{R,j,y}(t))\cdot\frac{(x(t),y(t))-(x_{R,j}(t),y_{R,j}(t))}{\|(x(t),y(t))-(x_{R,j}(t),y_{R,j}(t))\|}\Bigg] \end{aligned} \tag{4}$$

This establishes a relationship between Doppler and the state (position and velocity) of the target. Using a number of receivers (three or four) and an extended Kalman filter (Anderson & Moore, 1979; Moon & Stirling, 2000) using a Singer motion model (Singer, 1970), where the linearized version of (4) is used to form the observation equation, tracking can be achieved.

5. Some experimental results

The communication system, Doppler extraction, and extended Kalman filter algorithm were implemented and tested in a building. Figure 7 shows the layout of the building (The Sant Engineering Research Building on the campus of Utah State University). Receive antennas were placed at six locations in the ceiling of the building, of which four were used (at NW, SW, SC, and SE). The parameters of the hardware are described in Table 1. The parameters for the symbol timing synchronizer and PLL are shown in Table 2.

A target walked back and forth in the south hall (near the SW, SC, and SE antennas). To get an idea of what the Doppler frequency profile may look like, a simulation was created which approximates the Doppler frequency, with a simple model for human acceleration and deceleration at the ends of the traversals. This is not a high fidelity human motion model, but does help understand what the Doppler should be. An example of this for the SW antenna is shown in figure 8(a).

Figure 8(b) shows an actual extracted Doppler spectrum, using the MUSIC algorithm in conjunction with the Viterbi algorithm smoother.

From this system, the target trajectory was extracted. It was found that the reliability in the North/South direction was less than in the East/West direction, because there is only one antenna to distinguish N/S information. This led to variation in the extracted trajectory. This was then adjusted by taking the map of the building into account (targets cannot pass through walls). The resulting extracted trajectory is shown in figure 9. This track corresponds with the actual motion of the target.

6. Conclusions

Use of Gnu radio has enabled the implementation of a novel target tracking scheme which uses a digital communication system to create a bistatic radar scheme. By extracting the Doppler from the signal reflected from a moving target the trajectory of the target can be created.

Because of the low received signal power, the reliability of the estimated Doppler may be improved by using path-based algorithms such as the Viterbi algorithm or the BCJR algorithm.

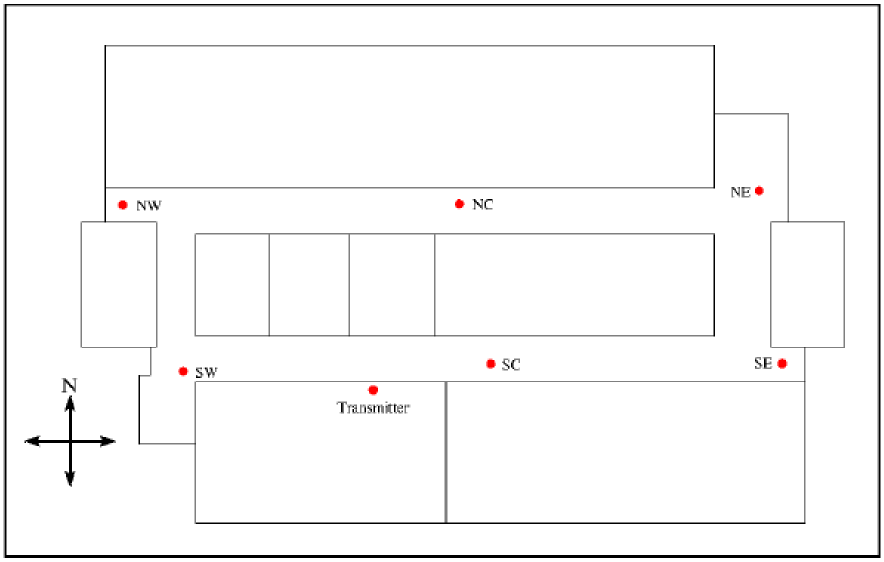

Figure 7. Antenna positions in building

References

Anderson, B. D. O. and Moore, J. B. *Optimal Filtering*. Prentice-Hall, Englewood Cliffs, NJ, 1979.

Bahl, L.R., Cocke, J., Jelinek, F., and Raviv, J. Optimal Decoding of Linear Codes for Minimizing Symbol Error Rate. *IEEE Trans. Info. Theory*, 20:284–287, March 1974.

Bradshaw, Thomas L. Alternative doppler extraction for indoor communication signals. Master's thesis, Utah State University, 2021.

Forney, Jr., G. David. The Viterbi Algorithm. *Proc. IEEE*, 61(3):268–278, March 1973.

Moon, Todd K. *Error Correction Coding: Mathematical Methods and Algorithms*. Wiley, 2005.

Moon, Todd K. and Stirling, Wynn C. *Mathematical Methods and Algorithms for Signal Processing*. Prentice-Hall, Upper Saddle River, NJ, 2000.

Schmidt, Ralph. Multiple emitter location and signal parameter estimation. *Proc. of the RADC Spectrum Estimation Workshop*, pp. 243–258, 1979.

Singer, Robert A. Estimating optimal tracking filter performance for manned maneuering targets. *IEEE Trans. Aerospace and Elect. Systems*, 6(4):473–483, July 1970.

Willis, Nicholas. *Bistatic Radar*. Artech House, 1991.

Table 1. Device Parameters

Transmitter	Ettus B200 mini
Transmitter gain	85 dB
Receiver 1	Ettus B210-1, RF A, TX/RX
Receiver 1 gain	45 dB
Receiver 1 antenna	SC
Receiver 2	Ettus B210-2 RF A, TX/RX
Receiver 2 gain	56 dB
Receiver 3	Ettus B200, TX/RX
Receiver 3 gain	80 dB
Number of amplifiers	2
Sample rate	62500 samples/s
Interp/Deci rate	4
Carrier Frequency	905 MHz

Table 2. Symbol Timing Synch/PLL parameters

Samples per symbol	8
Excess bandwidth	0.5
Matched filter length	161
TED	sgn(y[n]y'[n])
TED gain	1
Loop bandwidth	0.02
Damping factor	1.3
Maximum deviation	1.5
Interpolating resampler	MMSE, 8-tap, FIR
B_nT_s	90 m
ζ	0.707
K_p	0.5
K_0	1

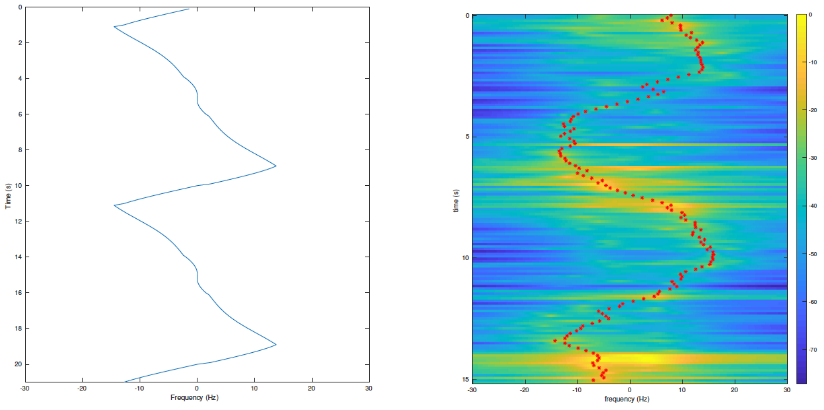

(a) Simulated Doppler trajectory

(b) Extracted Doppler

Figure 8. Simulated Doppler frequency at the SW antenna

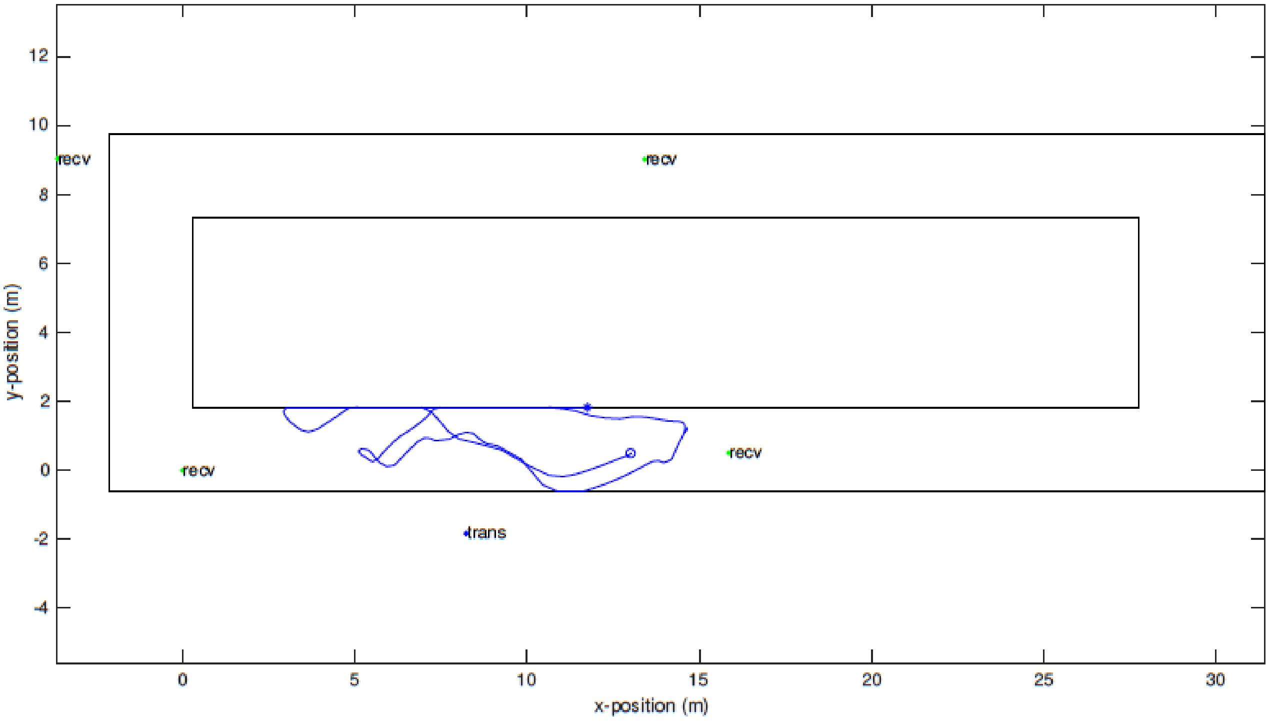

Figure 9. Motion tracking example